Demonstration of Integrated Longitudinal and Lateral Control for the Operation of Automated Vehicles in Platoons

Rajesh Rajamani, *Member, IEEE*, Han-Shue Tan, Boon Kait Law, and Wei-Bin Zhang

***Abstract*—This paper presents the design and experimental implementation of an integrated longitudinal and lateral control system for the operation of automated vehicles in platoons. The challenges handled in the design of the longitudinal control system include nonlinear vehicle dynamics, string-stable operation with very small inter-vehicle spacing, operation at all speeds from a complete stop to high-speed cruising, and the execution of longitudinal split and join maneuvers in the presence of communication constraints. The challenges handled in the design of the lateral control system include high-speed operation using a purely "look down" sensor system and lane changing without transitional lateral position measurements. The paper also describes the design of an on-board supervisor that utilizes inter-vehicle communication and coordinates the operation of the lateral and longitudinal controllers in order to execute entry and exit maneuvers. Extensive experimental results are included in the paper from the NAHSC[1] demonstration of automated highways conducted in August 1997 at San Diego, CA. The demonstration included a closely spaced eight-car platoon operating continuously over several weeks, with passenger rides being given to visitors. The maneuvers demonstrated included starting the automated vehicles from complete rest, accelerating to cruising speed, automated lane keeping, allowing any vehicle to exit from the platoon with an automated lane change, allowing new vehicles to join the platoon and bringing the platoon to a complete stop at the end of the highway.**

***Index Terms*—Automated highway systems, automated lane change, lateral vehicle control, longitudinal vehicle control, platoon.**

NOMENCLATURE

x_i	Longitudinal position of the ith vehicle.
$\dot{x}_i$ or v_i or v	Longitudinal velocity of the ith vehicle.
$\varepsilon_i = x_i - x_{i-1} + L$	Longitudinal spacing error of the ith vehicle, with L being the desired spacing.
v_ℓ	Longitudinal velocity of the lead vehicle of the platoon.
$\ddot{x}_\ell$	Longitudinal acceleration of the lead vehicle of the platoon.
C_1	Control gain used in upper longitudinal controller (relative weight for lead car signal feedback compared to preceding car signal feedback).
ω_n	Control gain used in upper longitudinal controller (bandwidth).
η_1, η_2	Sliding surface control gains.
$T_{\rm net}$	Net combustion torque of the engine.
T_{br}	Brake torque.
ω_e	Engine angular speed.
c_a	Aerodynamic drag coefficient.
R	Gear ratio.
h	Tire radius.
F_f	Rolling resistance of the tires.
J_e	Effective inertia reflected on the engine side.
$\dot{m}_{ai}$	Rate of mass flow into engine manifold.
$\dot{m}_{a0}$	Rate of mass outflow from engine manifold.
$\dot{m}_a$	Rate of air mass flow in engine manifold.
P_m	Pressure of air in engine manifold.
y_f, y_r	Lateral position error measurements at front and rear magnetometers respectively.
θ_v	Vehicle yaw angle.
ω_V	Vehicle yaw rate.
ω_R	Yaw rate contribution of the road.
C_f, C_r	Front and rear cornering stiffness, respectively.
I	Yaw moment of inertia.
m	Vehicle mass.
e_1	Lateral position error.
e_2	Yaw rate error.
δ	Steering angle.

I. INTRODUCTION

THE Automated Highway Systems (AHS) Program at California PATH[2] aims to reduce congestion on highways by achieving significantly higher traffic flow through closer packing of automatically controlled vehicles into platoons. The introduction of automation would also significantly improve safety, since studies have shown that over 90% of highway accidents occur due to driver-related human errors. Preliminary studies of automatic control of the longitudinal and lateral motion of cars were previously separately undertaken to establish feasibility of the AHS concept [1], [3], [13].

Manuscript received November 12, 1998; revised January 6, 2000. Recommended by Associate Editor, S. Banda.

R. Rajamani is with the Department of Mechanical Engineering, University of Minnesota, Minneapolis, MN 55455 USA.

H.-S. Tan and W.-B. Zhang are with California PATH, University of California, Berkeley, CA 94720 USA.

B. K. Law is with Open Telephone Network, Inc., Berkeley, CA 94704 USA.

Publisher Item Identifier S 1063-6536(00)05745-6.

[1]National Automated Highway Systems Consortium.

[2]California Partners for Advanced Transit and Highways.

This paper documents the integrated control system used in the NAHSC public demonstration in August 1997 of eight fully automated cars traveling together with small inter-vehicle spacing as a platoon. The demonstration was held in San Diego using a 7.6 mile segment of Interstate-15 HOV (car-pool) lanes. This section of the two-lane highway had been equipped with magnets installed in the centers of both lanes. The magnets served as reference markers that were used by the automated steering control system to keep each car centered in its lane. Over 1000 visitors were given passenger rides in the platoon vehicles which operated continuously for several hours a day for three weeks. The maneuvers demonstrated in San Diego included starting the automated vehicles from complete rest, accelerating to cruising speed, automated steering for lane keeping, allowing any vehicle to exit from the platoon with an automated lane change, allowing new vehicles to join the platoon and bringing the platoon to a complete stop at the end of the highway. These maneuvers are essential to an AHS.

This paper is organized as follows. Sections II and III describe the longitudinal and lateral control systems, respectively. Section IV describes the integration of the lateral and longitudinal systems and the design of an inter-vehicle coordination system. Section V presents detailed experimental results.

II. Longitudinal Control System Design

The hierarchical longitudinal control system developed at PATH for platooning consists of an upper level controller and a lower level controller. The upper level controller determines the desired or "synthetic" acceleration for each car in the platoon. The lower level controller determines the throttle and/or brake commands required to track the desired acceleration.

Sections II-A and II-B describe the longitudinal control system used for normal platoon operation. Section II-C describes the modifications needed to the normal longitudinal control system for performing entry and exit maneuvers (such as allowing any car to leave the platoon and allowing a car to join the platoon).

A. Upper Level Controller

The upper level controller determines the desired acceleration for each car so as to

1) maintain constant small spacing between the cars;
2) ensure string stability of the platoon (see explanation below).

As far as the upper level controller is concerned, the plant model used for control design is

$$\ddot{x}_i = u \tag{1}$$

where the subscript i denotes the ith car in the platoon. The acceleration of the car is thus assumed to be the control input. However, due to the finite bandwidth associated with the lower level controller, each car is actually expected to track its desired acceleration imperfectly. The performance specification on the upper level controller is therefore stated as that of meeting objectives 1 and 2 robustly in the presence of a first-order lag in the lower level controller performance

$$\ddot{x}_i = \frac{1}{\tau s+1}\ddot{x}_{i\_\mathrm{des}} = \frac{1}{\tau s+1}u_i. \tag{2}$$

Equation (1) is thus assumed to be the nominal plant model while the performance specifications have to be met even if the actual plant model were given by (2).

The spacing error for the ith vehicle is defined as $\varepsilon_i = x_i - x_{i-1} + L$ (please see nomenclature for notation). In terms of spacing error, the above objectives of the upper controller can be mathematically stated as follows:

1)
$$\varepsilon_{i-1} \to 0 \Rightarrow \varepsilon_i \to 0;$$

2)
$$\|\hat{H}(s)\|_\infty \le 1 \tag{3a}$$

where $\hat{H}(s)$ is the transfer function relating the spacing errors of consecutive cars in the platoon

$$\hat{H}(s) = \frac{\varepsilon_i}{\varepsilon_{i-1}}. \tag{3b}$$

The string stability of the platoon (objective 2, (3a)) refers to a property in which spacing errors are guaranteed not to amplify as they propagate toward the tail of the platoon ([4], [10]). For example, string stability ensures that any errors in spacing between the second and third cars does not amplify into an extremely large spacing error between cars 7 and 8 further down in the platoon. In addition to (3a), a condition that the impulse response function $h(t)$ corresponding to $\hat{H}(s)$ does not change sign is desirable [10], [11]. The reader is referred to [10] for details.

Longitudinal control algorithms that guarantee string stability in the platoon of vehicles include autonomous, semi-autonomous, and radio-communication-based algorithms. A comparison of the performance and deployment advantages of the three types of algorithms is provided in Rajamani [8]. The NAHSC demonstration implemented a radio communication-based algorithm described below.

The sliding surface method of controller design [9] is used. Define the following sliding surface:

$$S_i = \dot{\varepsilon}_i + \frac{\omega_n}{\xi + \sqrt{\xi^2-1}}\frac{1}{1-C_1}\varepsilon_i + \frac{C_1}{1-C_1}(v_i - v_\ell). \tag{4}$$

Setting

$$\dot{S}_i = -\lambda S_i \quad \text{with } \lambda = \omega_n(\xi + \sqrt{\xi^2-1}) \tag{5}$$

we find that the desired acceleration of the car is given by

$$\begin{aligned}\ddot{x}_{i\_\mathrm{des}} = {} & (1-C_1)\ddot{x}_{i-1} + C_1\ddot{x}_\ell \\ & - (2\xi - C_1(\xi + \sqrt{\xi^2-1}))\omega_n\dot{\varepsilon}_i \\ & - (\xi + \sqrt{\xi^2-1})\omega_n C_1(v_i - v_\ell) - \omega_n^2\varepsilon_i.\end{aligned} \tag{6}$$

The control gains to be tuned are C_1, ξ, and ω_n. The gain C_1 takes on values $0 \le C_1 < 1$ and can be viewed as a weighting

of the lead vehicle's speed and acceleration. The gain ξ can be viewed as the damping ratio and can be set to one for critical damping. The gain ω_n is the bandwidth of the controller.

Equation (5) ensures that the sliding surface converges to zero. If all the cars in the platoon use this control law, results in [10] and [11] show that the cars in the platoon are able to track the preceding car with a constant spacing and further that the system is string stable, i.e., the spacing errors never amplify down the platoon. Results on the robustness of the above controller, especially to lags induced by the performance of the lower level controller, can also be found in [10]. A wireless radio communication system is used between the cars to obtain access to all of the required signals. Each car thus obtains communicated speed and acceleration information from two other cars in the platoon—the lead car and the preceding car.

Setting $C_1 = 0$ for a two car platoon, we obtain the following classical second-order system:

$$\ddot{x}_{i\_\mathrm{des}} = \ddot{x}_{i-1} - 2\xi\omega_n\dot{\varepsilon}_i - \omega_n^2\varepsilon_i.$$

B. Lower Level Controller

In the lower controller, the throttle and brake actuator inputs are determined so as to track the desired acceleration described in (6). The following simplified model of vehicle dynamics is used in the development of the lower level controller. This simplified model is based on the assumptions that the torque converter in the vehicle is locked and that there is zero-slip between the tires and the road [4]. These assumptions relate the vehicle speed directly to the engine speed (see the Nomenclature for explanation of symbols)

$$\dot{x}_i = v_i = (Rh\omega_e)_i. \tag{7}$$

The dynamics relating engine speed ω_e to the pseudoinputs "net combustion torque" T_{net} and brake torque T_{br} can be then modeled by [4]

$$\dot{\omega}_e = \frac{T_{\mathrm{net}} - c_a R^3 h^3 \omega_e^2 - R(hF_f + T_{\mathrm{br}})}{J_e} \tag{8}$$

where $J_e = I_e + (mh^2 + I_\omega)R^2$ is the effective inertia reflected on the engine side, R is the gear ratio and h the tire radius.

$T_{\mathrm{net}}(\omega_e, m_a)$ is a nonlinear function of engine speed and mass of air in the intake manifold (obtained from steady-state engine maps available from the vehicle manufacturer). The dynamics relating m_a to the throttle angle α can be modeled as

$$\dot{m}_a = \dot{m}_{ai} - \dot{m}_{ao} \tag{9}$$

where $\dot{m}_{ai}$ and $\dot{m}_{ao}$ are the flow rate into the intake manifold and out from the manifold, respectively, and

$$\dot{m}_{ai} = \mathrm{MAX}\, TC(\alpha)\, \mathrm{PRI}(m_a) \tag{10}$$

where MAX is a constant dependent on the size of the throttle body, $TC(\alpha)$ is a nonlinear invertible function of the throttle angle and PRI is the pressure influence function that describes the choked flow relationship which occurs through the throttle valve. $\dot{m}_{ao}$ is the mass flow rate into the combustion chamber (again available as a nonlinear function of P_m and ω_e from the engine manufacturer). The ideal gas law is assumed to hold in the intake manifold

$$P_m V_m = m_a R_g T. \tag{11}$$

The control design for the lower level controller is based on a modification of the standard sliding surface control technique [9]. If the net combustion torque is chosen as

$$(T_{\mathrm{net}})_i = \frac{J_e}{Rh}\ddot{x}_{i\,\mathrm{des}} + \left[c_a R^3 h^3 \omega_e^2 + R(hF_f + T_{\mathrm{br}})\right]_j \tag{12}$$

then, from (8), the acceleration of the car is equal to the desired acceleration defined by the upper level controller: $\ddot{x}_i = \ddot{x}_{i\,\mathrm{des}}$.

Once the required combustion torque is obtained from (12), the throttle angle required to provide this torque is calculated by the following procedure. The pressure of air in the manifold P_m and temperature T are measured and m_a is then calculated using the ideal gas law (11). The map $T_{\mathrm{net}}(\omega_e, m_a)$ is inverted to obtain $m_{a\,\mathrm{des}}$.

A sliding surface controller [4] is then used to calculate the throttle angle α necessary make $m_{a\,\mathrm{des}}$ track m_a. Define the surface

$$s_2 = m_a - m_{a\,\mathrm{des}}. \tag{13}$$

Setting $\dot{s}_2 = -\eta_n s_2$, we obtain

$$\mathrm{MAX}\, TC(\alpha)\, \mathrm{PRI}(m_a) = \dot{m}_{ao} + \dot{m}_{a\,\mathrm{des}} - \eta_2 s_2. \tag{14}$$

Since $TC(\alpha)$ is invertible, the desired throttle angle can be calculated from (14).

If the desired net torque defined by (12) is negative, the brake actuator is used to provide the desired torque. An algorithm for smooth switching between the throttle and brake actuators is designed in [2] and will be used by the longitudinal control system.

C. Control System for "Split" and "Join" Maneuvers

In a realistic automated highway system, any car in the platoon should be allowed to take an exit at the request of its driver. This requires the exiting car as well as the car behind the exiting car to split to a larger spacing. Both these cars then switch to speed control during which the use of the radar for spacing control is suspended. The split to a larger spacing is necessary because close-spaced operation under purely speed control is unsafe. After the exiting car makes an automated lane change, the car behind it reverts back to spacing control and also speeds up to close the gap left by the exited car.

The communication hardware used for the NAHSC demonstration allowed the operation of only one platoon system at a time. To allow a car in the middle to make a lane change, the car behind it could not split and become the leader of a new platoon. Intra-platoon maneuvers were therefore designed to allow cars to execute split and join maneuvers in the platoon while still being a part of the platoon. The upper level controller of (6) is modified as follows during the split and join modes of operation.

Assume that the desired inter-car spacing is a slowly varying trajectory $L_i(t)$. Then for the splitting/joining car, the terms ε_i, $\dot{\varepsilon}_i$ should be calculated as functions of $L_i(t)$ and $\dot{L}_i(t)$. When the desired spacing is a function of time, the sliding surface

methodology of Section II leads to the following control law for desired acceleration:

$$\begin{aligned}\ddot{x}_{i\_\mathrm{des}} = {} & (1-C_1)(\ddot{x}_{i-1}-\ddot{L}_i)+C_1(\ddot{x}_\ell-\ddot{L}_i)\\ & -(2\xi-C_1(\xi+\sqrt{\xi^2-1})\omega_n\dot{\varepsilon}_i(\dot{L}_i,L_i)\\ & -(\xi+\sqrt{\xi^2-1}))\omega_n C_1(v_i-v_\ell+\dot{L}_i)\\ & -\omega_n^2\varepsilon_i(L_i). \end{aligned} \tag{15}$$

For the cars behind the splitting car, the terms associated with the preceding car speed and acceleration are independent of L_i, since it does fall back with respect to the lead car but does not fall back with respect to the preceding car. The control law for the cars behind the splitting/joining car is therefore

$$\begin{aligned}\ddot{x}_{i\_\mathrm{des}} = {} & (1-C_1)\ddot{x}_{i-1}+C_1(\ddot{x}_\ell-\ddot{L}_i)\\ & -(2\xi-C_1(\xi+\sqrt{\xi^2-1}))\omega_n\dot{\varepsilon}_i\\ & -(\xi+\sqrt{\xi^2-1})\omega_n C_1(v_i-v_\ell+\dot{L}_i)-\omega_n^2\varepsilon_i. \end{aligned} \tag{16}$$

The desired spacing for a split maneuver can be obtained from the following (relative) acceleration trajectories:

$$\begin{aligned}\ddot{L}_i(t) &= -\frac{a_0}{2}\{1-\cos(\omega t)\} \quad t<\frac{2\pi}{\omega}\\ \ddot{L}_i(t) &= \frac{a_0}{2}\{1-\cos(\omega t)\} \quad t\geq\frac{2\pi}{\omega}\end{aligned} \tag{17}$$

which ensures that both relative jerk and acceleration are zero at $t=0$ and $t=2\pi/\omega$. The variables a_0 and ω can be analytically calculated given the distance to split/join and either the maximum allowable relative velocity (a safety consideration) or the maximum allowable relative acceleration (an actuator consideration). For instance, given the maximum allowable relative acceleration a_0 and the distance to split H, $\omega=\pi\sqrt{2a_0/H}$ and the maximum relative velocity is $v_0=-\pi a_0/\omega$.

The intra-platoon maneuvers described above are valuable even when the communication hardware does not have the constraint described above and two platoons are able to operate in the same vicinity. This is because their accuracy and ride quality would provide superior and safer performance at small inter-car spacing compared to autonomous control on the splitting or joining car.

Note that the split/join maneuvers described above require communication from both the lead car and preceding car during the split/join and are performed as intra-platoon maneuvers. Communication is also required to coordinate the maneuvers between the cars in the platoon.

III. Lateral Control System

The basic functions of the lateral control system are lane-keeping and changing lanes when required. Discrete cylindrical magnets embedded in the center of the lane (typically every 1.2 meters apart) are used as reference markers by the lateral control system. Magnetometers mounted both on the front and rear of the car measure magnetic field intensity along three axes. The three-axis signal from each magnetometer is used to calculate the lateral distance from the center of the lane. The sensing algorithm and more details of the magnetic marker system can be found in [14]. By using magnetometers both in the front and rear of the vehicle, the yaw angle can also be computed and used in the control algorithm.

A. Lane-Keeping Controller

The fundamental challenge in the design of the lateral lane keeping system comes from the "look-down" characteristics of the magnetic marker sensing system, especially during high-speed driving conditions [3]. The two-degree of freedom model shown in Fig. 2 can be used to represent the dynamics of the vehicle lateral control system.

The two degrees of freedom of the vehicle are the lateral position y and the yaw angle θ_v. The equations of motion of the vehicle can be written in terms of error with respect to road coordinates as follows:

$$\begin{aligned}\frac{d}{dt}\begin{bmatrix}e_1\\ \dot{e}_1\\ e_2\\ \dot{e}_2\end{bmatrix} = {} & \begin{bmatrix}0 & 1 & 0 & 0\\ 0 & -\frac{c_f+c_r}{mv} & \frac{c_f+c_r}{m} & \frac{-c_f l_f+c_r l_r}{mv}\\ 0 & 0 & 0 & 1\\ 0 & \frac{-c_f l_f+c_r l_r}{Iv} & \frac{c_f l_f-c_r l_r}{I} & \frac{-c_f l_f^2+c_r l_r^2}{Iv}\end{bmatrix}\\ & \times\begin{bmatrix}e_1\\ \dot{e}_1\\ e_2\\ \dot{e}_2\end{bmatrix}+\begin{bmatrix}0\\ \frac{c_f}{m}\\ 0\\ \frac{c_f l_f}{I}\end{bmatrix}\delta+\begin{bmatrix}0\\ \frac{c_f l_f-c_r l_r}{mv}-v\\ 0\\ \frac{-c_f l_f^2-c_r l_r^2}{Iv}\end{bmatrix}\dot{\theta}_{\mathrm{des}}\end{aligned} \tag{18}$$

where $\dot{\theta}_{\mathrm{des}}=v/R$, $\ddot{e}_1=\ddot{y}+v\dot{\theta}_v-v\dot{\theta}_{\mathrm{des}}$ represents the lateral acceleration error with respect to the road center-line and $e_2=\theta_v-\theta_{\mathrm{des}}$ represents yaw error with respect to the road. The parameters are described in the Nomenclature.

Note that the lateral dynamics model shown above is a function of the longitudinal vehicle speed v. Results from [3] show that the damping in the transfer functions from δ to lateral position measurement reduces as the vehicle longitudinal speed increases. The damping of the "zeros" of the lateral system reduces more dramatically than that of the poles when the lateral measurement is taken at locations close to the front of the vehicle (as in a typical "look-down" lateral sensing system). The combination of bad poles and worse zeros creates a difficult control problem especially when high controller gain is required and practical steering actuator limitations are imposed. Any high gain controller tends to drive the closed-loop poles toward the open-loop zeros, resulting in poorly damped closed-loop poles. A perfect pole–zero cancellation is impossible because of system parameter uncertainties. The lightly damped poles introduced by the controller would show up in yaw dynamics, uncancelled. This would result in excessive fish-tailing of the vehicle at high speeds.

The study in [3] concluded that the best control strategy is to use an additional sensor at the tail end of the vehicle in a so-called "virtual" look-ahead concept. Complementing a lateral displacement sensor at the front bumper by this second sensor allows forward extrapolation to a virtually increased look-ahead distance beyond the vehicle boundaries. In practice, the amplification of measurement noise limits the virtual look-ahead to just a few vehicle lengths.

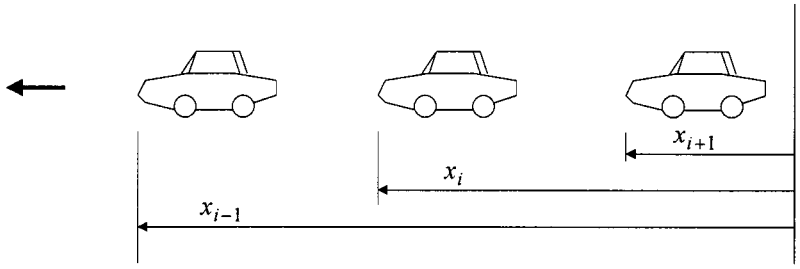

Fig. 1. Platoon of cars—upper controller notation.

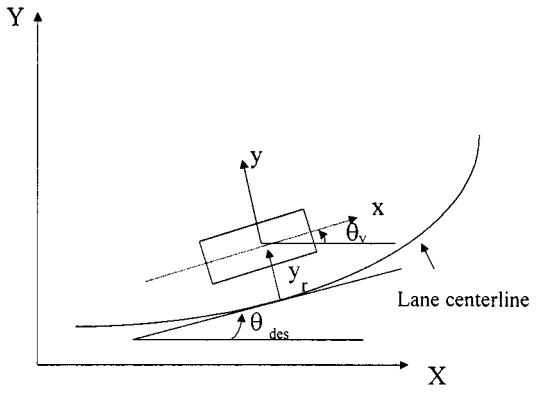

Fig. 2. Lateral vehicle dynamics.

The following frequency shaped virtual look-ahead lane-keeping control algorithm was developed for use in the NAHSC demonstration vehicles:

$$\delta = -k_c G_c(s)\{(k_{\text{int}} + k_e k_{\text{ext}})y_f - k_e k_{\text{ext}} y_r\} \tag{19}$$

where k_{int} is the integrator at the front sensor location, k_{ext} the virtual sensor extension filter, G_c is the compensator at the virtual sensor location, k_e and k_c are gain constants, $y_f = e_1 + \ell_f e_2$ and $y_r = e_1 - \ell_r e_2$ are the lateral measurements at front and rear sensors, respectively. This controller consists of three elements: 1) an integral control that keeps the steady-state tracking error at the front sensor to be zero; 2) a frequency shaped look-ahead distance that provides more look-ahead distance at frequencies around the vehicle lateral modes and rolls off the look-ahead distance at higher frequencies; and 3) a servo controller that uses the frequency shaped virtual displacement as input and compensates for the actuator and suspension dynamics.

A gain-scheduling scheme is incorporated into the lane-keeping control algorithm to provide a better tradeoff between passenger comfort and tight tracking control, especially in view of the misalignments that exist in the magnet markers. The gain-scheduling is done through the parameter k_c. The magnitude of the gain is changed in such a way that decreasing steady-state gain comes with increasing virtual look-ahead distance. A built-in hysteresis, that is applied only when the controller gain is reduced is employed to eliminate excessive switching. High gain is used in the following situations: low vehicle speed, large tracking error, large lateral acceleration, and large curvature if the information is known. Otherwise low gain is used.

B. Lane-Change Controller

The purpose of the automated lane change controller is to automatically steer the vehicle from the current lane to an adjacent lane. The fundamental difference between using look-down and look-ahead sensors for this task is the difference in the range of the lateral sensors. Look-ahead sensors typically have larger sensor range. Lane change and lane keeping maneuvers become virtually identical when the lateral sensor can measure its location with respect to both lanes. The control problem becomes more complicated when the lateral sensor can not sense both lanes and the vehicle must travel a certain distance without seeing the road reference markers. In this case, the difficulty of conducting an automated lane-change maneuver increases proportionally with the inverse of the lateral sensor range and directly with the vehicle longitudinal velocity square (see [12]).

Two schemes of lane change maneuvers by using roadway marker reference systems have been developed at PATH [12]: infrastructure guided lane change and automated free lane change. In the infrastructure guided lane change scenario, additional magnetic markers are installed between lanes to provide a reference path for automatically guided vehicles at certain locations on the highway. This scheme alleviates the control and estimation issues but limits lane change maneuvers to specific locations on the highway. On the other hand, in the free lane change scenario, vehicle position during the lane change is estimated from yaw rate measurement and a smooth trajectory is generated as a virtual reference path for the vehicle to follow in between lanes. Experimental results on highway I-15 have demonstrated the feasibility of both approaches up to speeds of 80 mi/h.

1) Infrastructure Guided Lane Change: In the case of the infrastructure guided lane change, a line of road markers is installed in between two lanes of the roadway designated for lane change (see Fig. 3 for illustration). This additional marker line is designed to guide the automated lane change maneuver from the traveling lane to the target lane. However, sensor limitation or field interference often requires certain minimum spacing between marker lines. For instance, magnetic marker lines can not be installed too close to each other to avoid field interference. In such a situation, an open-loop steering command may be used to bridge the gap between the two marker lines without the help of additional sensors. Dead reckoning based on inertial sensors can also be incorporated for added robustness.

The major complexity in the execution of an infrastructure guided lane-change results from the many controller states involved in any lane change maneuver. Assuming the automated

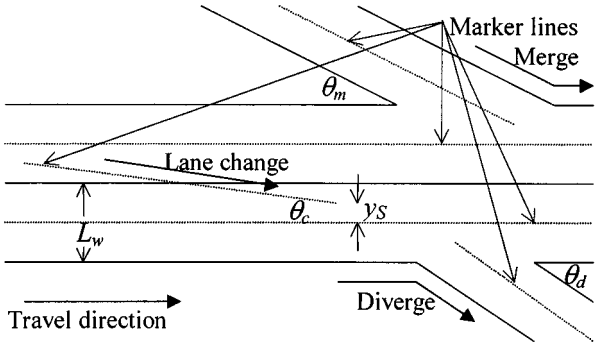

Fig. 3. Infrastructure guided lane change.

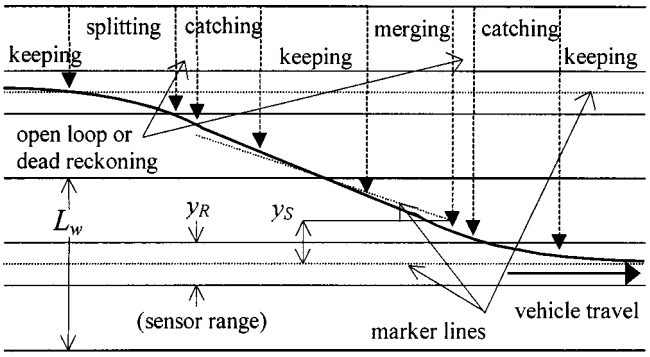

Fig. 4. Controller states for infrastructure guided lane change.

vehicle starts from a normal lane keeping function, the infrastructure guided lane change maneuver is composed of the following controller states with the sequence shown in Fig. 4.

1) Lane-splitting: the automated vehicle follows a prescribed trajectory until it leaves the sensor range of the main marker line.
2) Open loop/dead reckoning: the automatic vehicle uses either a prescribed open-loop steering command or follows a predetermined trajectory based on dead reckoning estimation of lateral displacement until it reaches the guided marker line.
3) Lane-catching: the automatic vehicle determines how to resume the lane keeping control based on how the vehicle first encounters the new line.
4) Lane-keeping: once latches on to the guided marker line, the automatic steering control starts the normal lane keeping control function along the guided lane-change marker line.
5) Lane-merging: the automated vehicle follows a prescribed trajectory with the help of the marker line to properly position itself for the incoming "open-loop" operation.
6) Open loop/dead reckoning: after reading the last marker of the infrastructure guided line, the automatic vehicle again uses a predetermined open-loop steering command or follows a virtual trajectory based on dead reckoning to search for the target lane.
7) Lane-catching: once the lateral sensor reads the markers from the target lane, the automatic algorithm determines and follows a trajectory that transitions the vehicle to the normal lane keeping function on the target lane.
8) Lane-keeping: the vehicle resumes normal line keeping control along the marker line of the target lane.

The design of the automated infrastructure guided lane change maneuver involves development of the following four components: 1) trajectory planning; 2) open-loop steering command or dead reckoning estimation; 3) controller state machine; and 4) lane-keeping controller.

There are three trajectories that need to be defined during an infrastructure guided lane change maneuver: lane splitting, lane merging, and lane catching. Third-order polynomials have been chosen for the above scenarios because of the relatively simple real time computation. Because the infrastructure guided lane change maneuvers are conducted based on the preinstalled marker locations, the trajectories are defined as functions of longitudinal positions as shown (20). The vehicle tracks $y = y_d(x)$ instead of road center $(y = 0)$ as the vehicle follows the desired trajectory

$$y_d(x) = a_3x^3 + a_2x^2 + a_1x + a_0 \tag{20}$$

with

$$\begin{aligned} a_0 &= y_d(0), \\ a_1 &= \dot{y}_d(0) = \frac{dy_d}{dx}(0) \\ a_2 &= -\frac{2(y_d(x_f) - y_d(0))}{x_f^3} + \frac{\dot{y}_d(x_f) + \dot{y}_d(0)}{x_f^2} \\ a_3 &= \frac{3(y_d(x_f) - y_d(0))}{x_f^2} - \frac{\dot{y}_d(x_f) + 2\dot{y}_d(0)}{x_f}. \end{aligned} \tag{21}$$

The longitudinal position, x, starts at zero for simplicity. The parameter x_f defines the length of the trajectory. Table I shows a typical application of (20) and (21) to lane splitting, merging, and catching scenarios. The length of the trajectory, x_f, can be chosen between 20 m and 40 m. ψ is an additional trajectory angle whose value depends on the system noise level. The lane-catching trajectory depends on the initial states $(y(t_a), \theta_a)$ as the vehicle first encounters the new marker line.

The open-loop steering command uses the low-pass filtered value of the steering command during the final stage of lane-splitting or lane-merging. The controller state machine determines the transitions among controller states based on the inputs from the lateral sensors, the travel plan, and the information of where the lane change guided lines are. The lane-keeping controller described by (19) is strong enough to be used as the trajectory following controller for the lane-change.

2) Automated Free Lane Change: The major difficulty in an automated free lane change is the extreme sensitivity of the system to yaw-rate sensor noise. This sensitivity arises due to the low yaw-rate levels associated with typical lane change operations. The automatic free lane change control algorithm consists of four components that work closely with each other. They are:

1) a lateral displacement observer/estimator that uses yaw rate sensor (and/or accelerometer);

TABLE I
TRAJECTORY PLANNING

	$y_d(0)$	$\dot{y}_d(0)$	$y_d(x_f)$	$\dot{y}_d(x_f)$
lane-split	0	0	$-y_S$	$\theta_c + \psi$
lane-merge	0	0	y_S	$-\theta_c - \psi$
Lane-catch	$y(t_a)$	θ_a	0	0

2) a trajectory planning scheme that determines lane-change and lane-catching trajectories;
3) a robust lane-keeping control algorithm that can bring the vehicle to road center even at large arriving angles;
4) a state machine that coordinates the above three components based on sensor signals, road information, and maneuver demands.

During the free lane change maneuver, the estimator determines the lateral displacement based on the yaw rate measurement when there are no markers in between lanes. Since the lateral displacement is roughly a double integral of the yaw rate measurement, it is sensitive to any bias. There are three major sources of such biases 1) the yaw rate sensor bias or drifting; 2) the road geometrical yaw rate contribution during curving on the roadway; and 3) errors in the estimate of the initial conditions as the vehicle leaves the marker line. Equation (22) describes the estimate $\hat{y}$, where y_0, θ_0, and ω_0 are the initial condition or bias of lateral displacement, vehicle angle, and yaw rate, respectively.

$$\hat{y} = \hat{y}_0 + V\hat{\theta}_0 t + \frac{1}{2}V\hat{\omega}_0 t^2 + V\iint \omega\, dt. \tag{22}$$

The basic procedure is to first estimate the initial conditions and bias in (22) when the lateral measurements are available. As the vehicle exits the sensor range, (22) would be used for dead reckoning computation of $\hat{y}$. Equation (22) also implies a strong requirement to the displacement estimator. For example, the errors of the estimates of θ_0 and ω_0 should not exceed 0.13° and 0.085°/s, respectively if their individual contribution to the displacement error is less than 0.2 m, with $V = 30$ m/s and $t = 3$ s. To satisfy such strong requirements, we use kinematic relationships for estimator design, since they are more reliable than the dynamic characteristics. The vehicle traveling at angle θ_V can be described as

$$\dot{\theta}_V = (\omega_V + \omega_R) \tag{23}$$

where ω_V and ω_R are the true vehicle yaw rate and the yaw rate contribution of the road, respectively. The vehicle angle estimator $\hat{\theta}$ can then be written as

$$\dot{\hat{\theta}}_V = \omega_M + K_e(\bar{\theta}_V - \hat{\theta}_V) \tag{24}$$

with

$$\omega_M = \omega_V + \omega_N, \quad \text{and} \quad \bar{\theta}_V = \theta_V + \theta_n$$

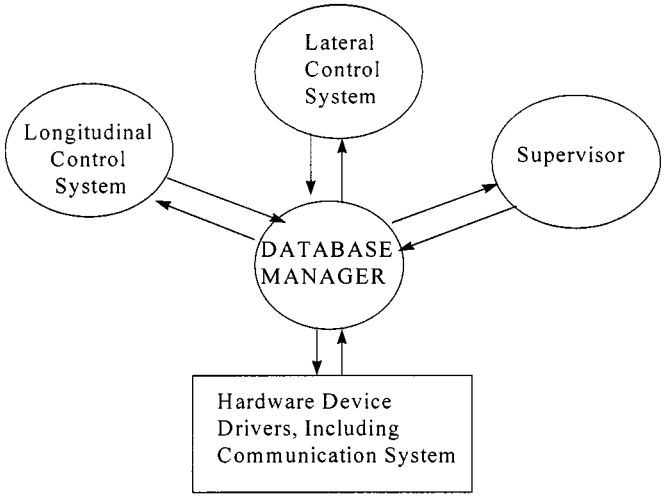

Fig. 5. Structure of integrated real-time software.

where ω_N is the measurement noise and bias of the yaw rate sensor, and $\bar{\theta}_V$ is the computed value of θ_V, with θ_n the computational noise. From (23) and (24), we obtain

$$K_e(\bar{\theta}_V - \hat{\theta}_V) = \frac{K_e}{s + K_e}(\omega_R - \omega_N) + \frac{K_e s}{s + K_e}\theta_n. \tag{25}$$

Since $\omega_R - \omega_N$ is exactly the yaw rate "bias" that should be used when the vehicle leaves the lateral sensor range, the low-pass filtered value of $K_e(\bar{\theta}_V - \hat{\theta}_V)$ provides a good estimate for the yaw rate bias. To reduce the impact from θ_n, the bandwidth of the low-pass filter is chosen to be about $K_e/10$. A similar technique can also be applied to the kinematic relationship between y and θ_V.

Lane change reference trajectories play a crucial role in the lane change maneuver. There are two trajectories that need to be designed: 1) lane-change trajectory: the trajectory that the vehicle follows to leave the first lane and to perform the lane change maneuver until the lateral sensor picks up the markers at the target lane and 2) lane-catching trajectory: the trajectory the vehicle follows from the time the sensor sees the target lane till the vehicle aligns to the new marker line. Both third- and fifth-order polynomials as described in Section III-B1 can be used for the lane-change/catching trajectory. The lane-change trajectory is adaptive to vehicle speed so that the time of dead-reckoning is about 3–5 s.

IV. INTEGRATED SYSTEM OPERATION

The longitudinal and lateral control systems described in the previous two sections were developed independently. For the fully automated cars, while the basic lane keeping and longitudinal spacing control can be performed independently, coordination between the two controllers is required to perform maneuvers like exit from the platoon, entry, etc. A coordinated response is also required in the event of sensor or actuator malfunctions where a fault handling action has to be taken.

Both the lateral and longitudinal control systems were implemented as independent processes in the real-time software. The structure of the real-time software is shown in Fig. 5 and was implemented in the real-time operating system QNX. The

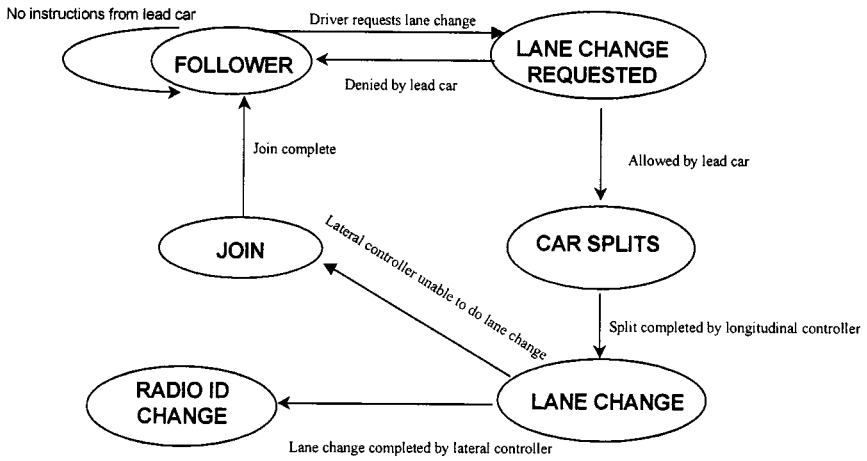

Fig. 6. Finite-state machine for supervisor of car requesting an exit.

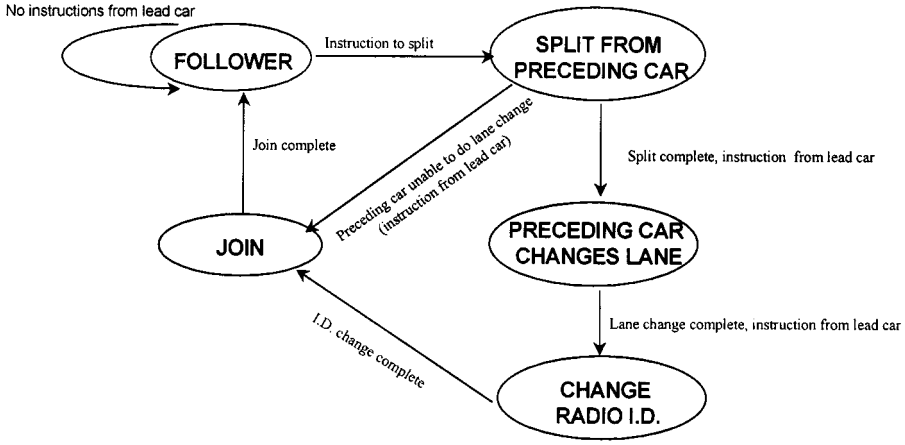

Fig. 7. Finite-state machine for supervisor of vehicle behind exiting car in platoon.

three other important processes shown in Fig. 5 are the database manager, the supervisor, and the hardware device drivers. The four processes: longitudinal control system, lateral control system, device drivers, and supervisor communicate with each other through the memory locations maintained by the database manager. QNX allows different sampling times and priorities to be assigned to different processes.

The supervisor shown in Fig. 5 is an important process that coordinates the maneuvers to be performed by the lateral and longitudinal control systems. It retrieves magnet marker location, the status of the maneuver from the lateral and longitudinal systems as well as inputs from the driver of the car through the database. Based on these inputs, the supervisor prescribes a desired maneuver for both the lateral and longitudinal controllers using the finite state machines described below.

Figs. 6 and 7 describe the process of a lane change and the coordination actions performed by the supervisor for the same. Fig. 6 shows the state machine for a car when the driver has requested an exit from the platoon while being a follower. The request is transmitted to the lead car which grants permission only if all the other cars in the platoon are in the FOLLOWER state and have not requested an exit. While granting permission to the car to exit, the lead car also instructs the car behind it to SPLIT (Fig. 7). This is necessary because the car behind the lane changing car has to suspend use of radar and operate open-loop while the lane change takes place. When both the exiting car and the car behind have completed splitting, the lead car grants permission to do the lane change. If the requesting car is unable to do a lane change (for example, due to cars in the other lane on a real highway), it informs the lead car and then moves to the JOIN state. After the join is completed, the car comes back to the FOLLOWER state. In this case the lead car instructs the following car also to move to the JOIN and then FOLLOWER states.

If the requesting car successfully performs a lane change, it changes its Radio I.D. to become the last car in the platoon (In an actual AHS it would cease to be a part of the platoon). All the cars behind decrement their Radio I.D. The car behind then moves to the JOIN and then FOLLOWER states.

While in the SPLIT and JOIN states, the desired acceleration is determined by (15), and (17) as derived in this section. The cars in the platoon behind the splitting/joining cars use the desired acceleration maneuver of (16).

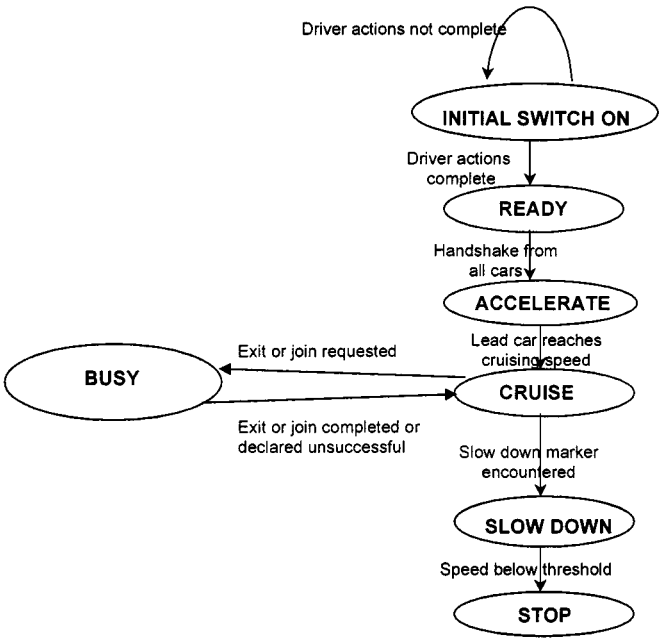

Fig. 8. Finite-state machine for the lead car in the 1997 NAHSC Demonstration.

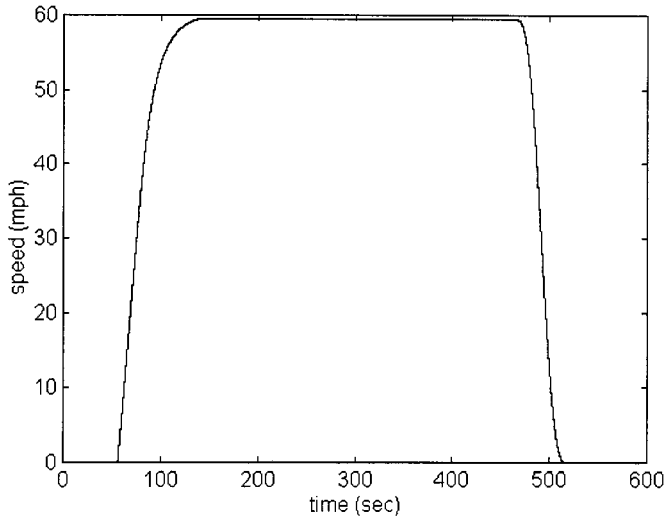

Fig. 9. Desired speed profile for lead car.

To complete the description of the integrated automated vehicles, the following list of major components on the vehicles is provided below:

- Magnetometers, specified by PATH and manufactured by Applied Physics of Mountain View, CA, detected lateral position relative to each magnetic marker and read the road information encoded in the markers.
- Steering actuator, designed by Delphi Saginaw, used a small motor and encoder assembly attached to the steering column to turn the steering wheel.
- Brake actuator, developed by Delphi Chassis, was a modification to the existing ABS system.
- Throttle actuator, designed by PATH and installed by General Motors, used a stepper motor to drive the throttle position that provides the desired acceleration.

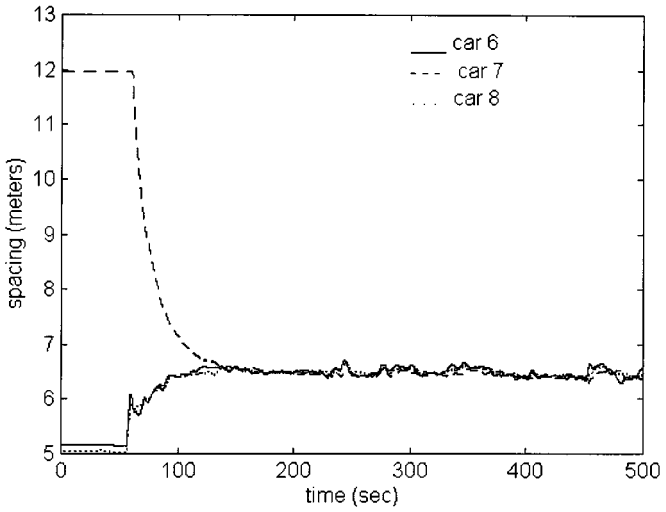

(a)

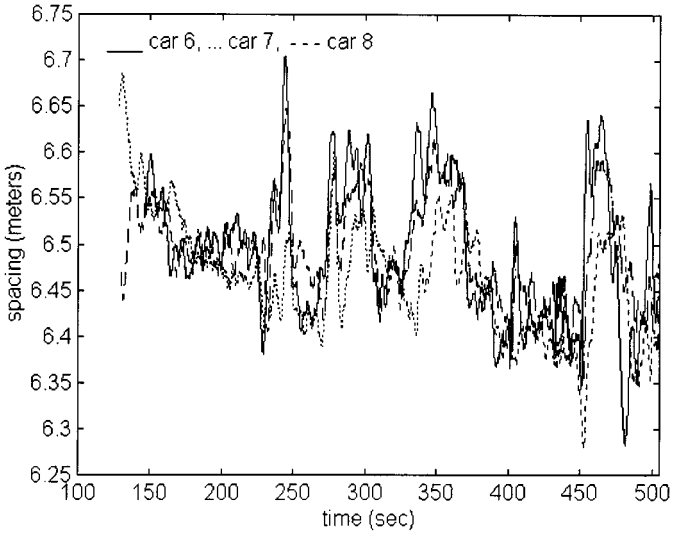

(b)

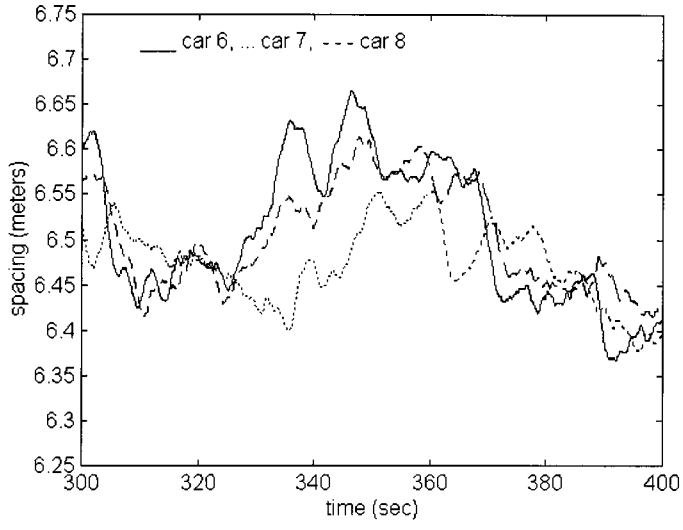

(c)

Fig. 10. Spacing performance of cars 6, 7, and 8 of the eight-car platoon (a) raw radar; (b) estimated inter-car spacing; (c) estimated inter-car spacing.

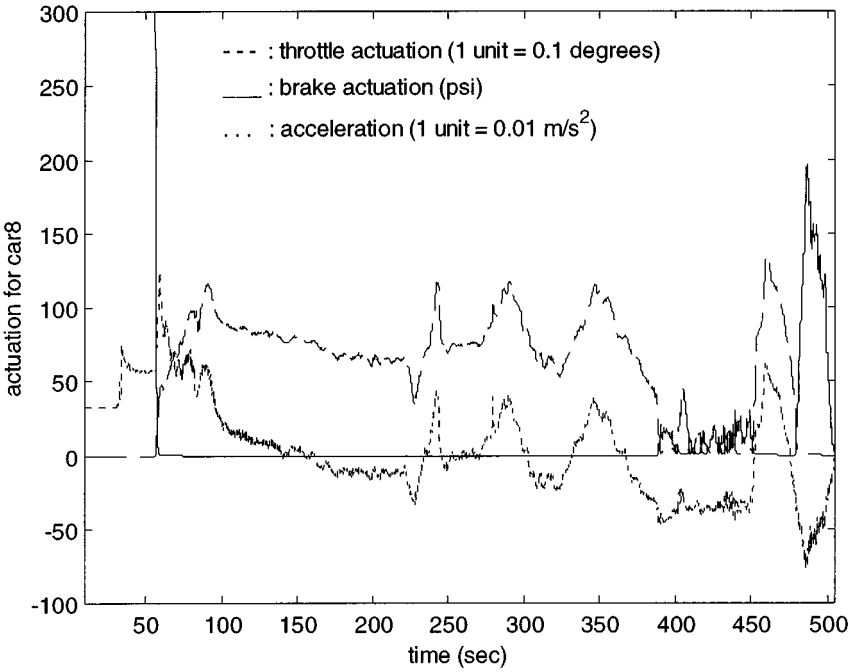

Fig. 11. Desired acceleration, throttle, and brake for car eight.

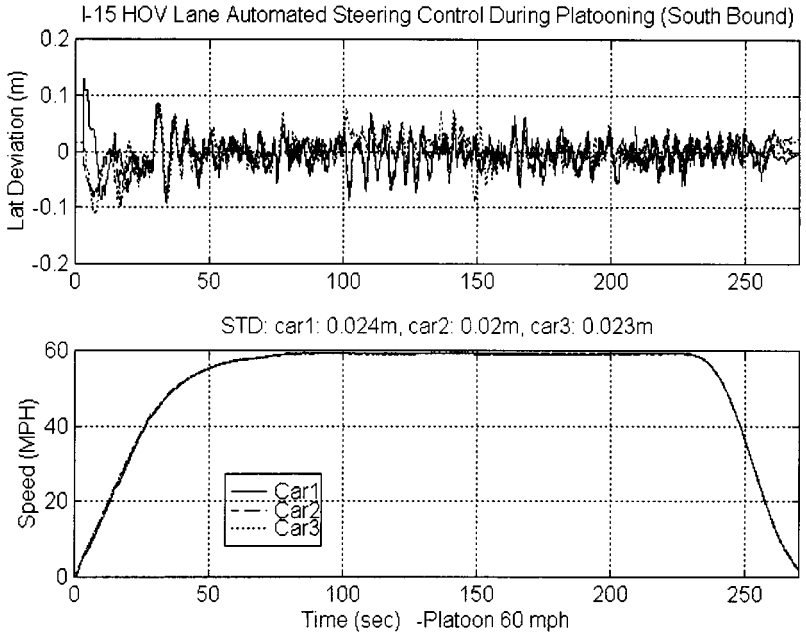

Fig. 12. I-15 automated steering control during platooning.

- Pentium computer, a industrial grade desktop with heavy-duty chassis in the trunk, provided intelligence to the automated system.
- Human machine interface computer, developed by Delco Electronics, provided screen images based on commands from the control computer.
- Data radio link, developed by Utilicom for Hughes, enabled real-time data communication between vehicles in the platoon.
- Heads-up display, developed by Delco Electronics, provided the driver with vehicle lateral and longitudinal measurements and other information.
- Panel display, developed by Delco Electronics, informed the driver of the system operation status and upcoming maneuvers.
- Internal state sensors, like engine speed, manifold pressure and yaw-rate sensors used by the control systems, were installed by General Motors Research.

V. Experimental Results from the NAHSC Demonstration

Eight GM Buick Le Sabres were used in the August 1997 NAHSC demonstration. The demonstration was held in San Diego using a 7.6-mi two-lane highway that had been equipped with magnets installed in the centers of both lanes. The magnets served as reference markers that were used by the automated steering control system to keep each car centered in its lane. Visitors were given passenger rides in the platoon vehicles which operated continuously for several hours a day for three weeks. The objective of this demonstration was to show that cars could travel in a platoon safely and comfortably and also that each car in the platoon could take an exit anytime at the request of its driver.

The finite state machine describing the discrete event response of the lead car during the run is shown in Fig. 8. The scenario in each demonstration run is described below. All of the eight cars start together from rest at arbitrary initial inter-car spacing (INITIAL SWITCH ON). The driver of each car turns on the automation switches and moves the gear from park to drive. The automatic controller applies brakes to keep the car stationary. It checks to see if all of the driver actions have been correctly completed. Then the car transitions to the READY state where it sends out a handshake communication message to the lead car of the platoon. Once the lead car receives handshake messages from all of the cars in the platoon it sends out the ACCELERATE command to all the cars in the platoon. The cars accelerate together until they reach a cruising speed of 60 mi/h with a steady-state inter-car spacing of 6.5 m between them (CRUISE/FOLLOWER). Once the CRUISE state has been reached, any car in the platoon can request a lane change. The coordination between the cars in this case has been described in Section IV.

Finally, when the lead car passes a coded magnetic marker in the lane which indicates that the end of the 7.6-mi highway is approaching, it moves to the SLOW DOWN state. All of the cars decelerate together and maintain their 6.5-m spacing even as they come to a complete stop (STOP).

The lead car of the platoon does not allow more than one exit request to be permitted in the platoon (it allows one exit only when all cars in the platoon are in the CRUISE/FOLLOWER state). Once a car in the platoon has been given permission to exit, no other car in the platoon is allowed permission to exit until all cars are back in the CRUISE/FOLLOWER state. The above scenario described a fault-free operation where the only failure allowable is failure to execute the lane change.

The following figures document the performance achieved during the August 1997 NAHSC Demonstration. Fig. 9 shows the desired speed trajectory for the lead car of the eight-car platoon. The desired speed trajectory starts from zero speed, ramps up, and then smooths out exponentially before cruising at approximately 60 mi/h. The desired trajectory stays constant at 60 mi/h until the user-specified magnetic marker is reached to start decelerating to a stop. The deceleration to a stop is achieved using a speed profile consisting of a ramp combined with a sinusoid. In the acceleration and deceleration trajectories, two gear changes (1 to 2 and 2 to 3) take place in the automatic transmission system.

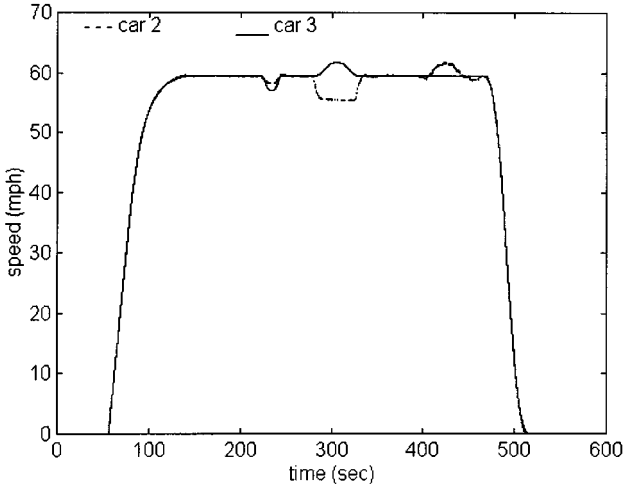

Fig. 13. Speed profiles of cars 2 and 3 in the platoon.

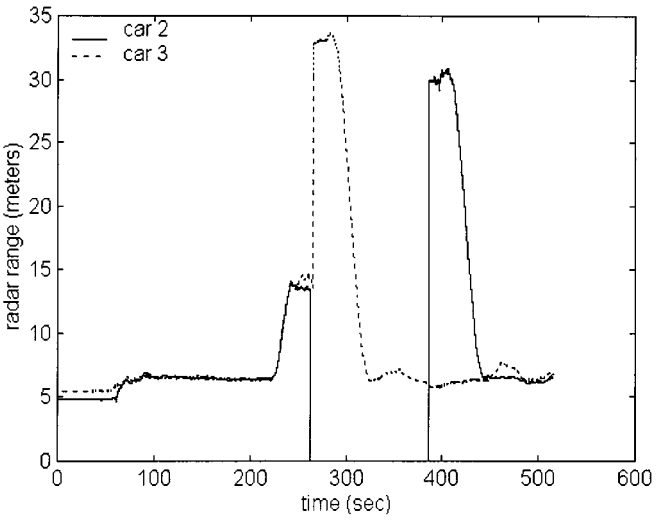

Fig. 14. Spacing performance of cars 2 and 3 of the eight-car platoon (raw radar).

Fig. 10(a)–(c) shows the spacing performances of cars 6, 7, and 8 which form the tail of the eight-car platoon. The cars start with arbitrary initial spacing. The steady-state desired spacing between the cars is 6.5 m. During the entire 7.6-mi run on the San Diego highway, the spacing error between these tail vehicles of the platoon remains within ± 0.2 m. This includes the spacing performance while the lead car accelerates, cruises, decelerates to a complete stop, and other cars accelerate and decelerate while splitting and joining. The scenario also includes steep uphill and downhill grades during which the maximum spacing error occurs. Fig. 10(a) shows the initial arbitrary spacing between cars during start-up and the convergence to the steady-state 6.5-m spacing. Fig. 10(b) and (c) shows close-ups of the inter-car spacing to indicate the accuracy and smoothness of the longitudinal controller.

Fig. 11 shows the desired acceleration, throttle, and brake actuation for car eight. Initially all the cars are at rest and the brake actuator maintains 300 lb/in^2 pressure in the master cylinder to

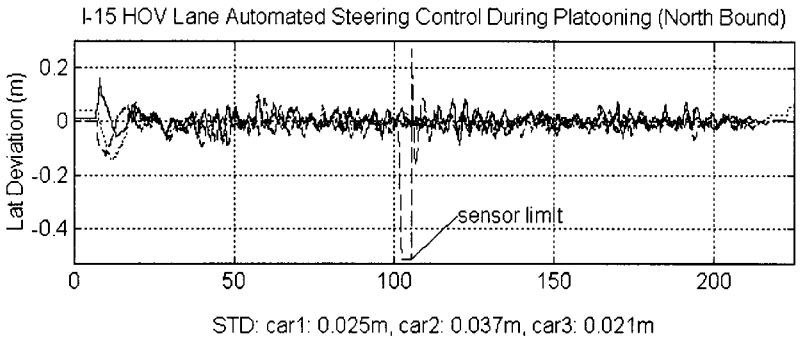

Fig. 15. I-15 automated lane-keeping and lane-change during platooning.

keep the car stationary. The throttle angle of the actuator stays at zero. During the initial acceleration maneuver of the platoon, the throttle angle increases to as much as 12°. The maximum value in throttle angle is required during the gear change from gear 1 to gear 2 which takes place during an uphill ascent on the highway. The steady state throttle angle during cruise on flat ground is less than 10°. The variations in throttle angle due to steep uphill and downhill grade variations are also seen in the figure. At approximately 475 s, the cars begin to decelerate to stop and the throttle angle then gradually drops to zero. The brake actuator is mostly not used once the car starts moving, except at the very end of the 7.6-mi highway during the downhill and during the deceleration maneuver. During the final deceleration to a stop maneuver, the car decelerates at 0.05 g which translates into a maximum braking pressure requirement of about 200 lb/in^2. This figure illustrates the use of both actuators and the smooth switching between them for conducting all the maneuvers described in the demonstration scenario.

Fig. 12 shows the performance of the lane-keeping control during a platoon run with no lane change at 60 mi/h for car 6, car 7 and car 8. The standard deviations of the tracking error for car 6, car 7, and car 8 are 2.4, 2.0, and 2.3 cm, respectively. The tracking errors are within 7.5 cm over 99% of the time. Furthermore, the tracking errors of these three cars are very similar at every location, demonstrating the consistency of the automated steering control system.

During the run in Fig. 10, car 2 requests and performs a lane change to exit from the platoon. Fig. 13 shows the speed profiles and Fig. 14 shows the inter-car spacing variation for cars 2 and 3 of the platoon. At approximately 225 s, the driver of car 2 requests an exit from the platoon. In response, car 2 splits smoothly to a larger spacing of 13.5 m. Simultaneously, car 3 is also commanded by the lead car to split to a spacing of 13.5 meters with respect to car 2. After the two split maneuvers are complete, at approximately 265 s, car 2 makes an automated lane change. Since car 2 no longer has a preceding car that it can track or any other target, its spacing as measured by the radar drops to zero. The spacing as measured by the radar on car 3 increases to 34 m. Once car 2 indicates via radio communication that it has completed its lane change, car 3 then initiates a join maneuver and decreases the spacing between itself and car 2. The steady-state spacing between car 3 and car 1 comes back smoothly to 6.5 m. Car 2 decelerates to the tail of the platoon in the other lane and then makes a lane change to come back to the original lane. Its radar measurement reads 31 m when it comes back to the original lane. It then initiates a join maneuver and joins with car 8 to decrease its final spacing to 6.5 m. The speed profile of car 2 shows the maneuvers accelerate, cruise, split, lane change, fall back, join, and decelerate. The speed profile of car 3 shows accelerate, cruise, double split, join, and decelerate.

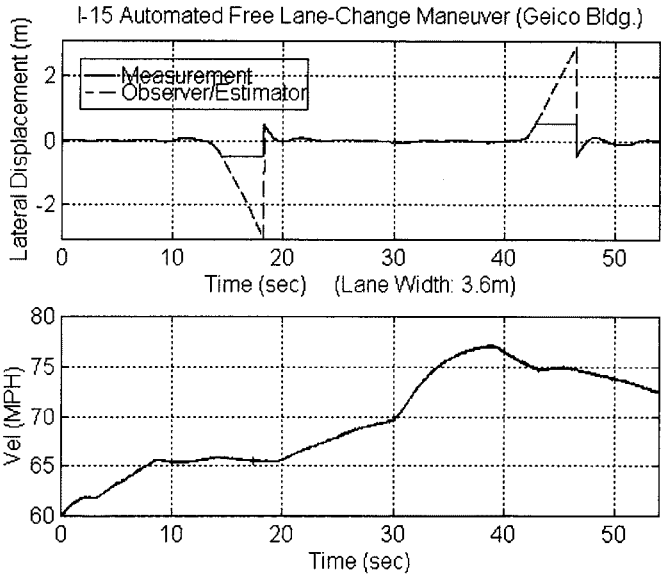

Fig. 16. I-15 high-speed lane-change during testing.

Fig. 15 summarizes the lane keeping and lane change performance of cars 1, 2 and 3. As described earlier, car 2 in this run requests a lane change and automatically steers to the adjacent lane after completing splitting. The standard deviations of the tracking errors are 2.5, 3.7 and 2.1 cm. The larger error of car 2 is created during the lane change where the vehicle leaves the original sensor range and catches a new lane, as can be observed in Fig. 15.

Fig. 16 illustrates the lateral control performance of the automated free lane change maneuver in more detail. Two consecutive free lane changes were recorded in this test data, the first at 65 mi/h and the second at 75 mi/h with steering control under automation, but with the driver controlling the throttle and brake. The figure compares the lateral displacement measurement and its estimation. As the vehicle reaches the limit of the sensor range (0.53 and -0.52 m), the estimator readings were at -3.11 and 2.93 m, respectively, for the two lane changes.

These numbers indicate that the accuracy of the two estimates are within 0.15 m since the lane width is 3.6 m. The estimator's errors are less than 0.35 m as the vehicle reaches the target lane at about 3.6 m away from the initial lane.

VI. Conclusion

As a part of the National Automated Highway System Consortium (NAHSC) demonstration held in August 1997, an automated eight car platoon was demonstrated in San Diego, with many visitors being given demonstration rides over a 7.6-mi highway. The eight-car platoon was demonstrated with continuous operation for 6–8 h each day and for three weeks in a row. The control system had the reliability and robustness necessary for such continuous operation. This paper documented the lateral and longitudinal control systems used in the demonstration as well as the coordination system between the two controllers and between cars in the platoon in order to perform important entry-exit maneuvers. The maneuvers demonstrated included starting the automated vehicles from complete rest, accelerating to cruising speed, allowing any vehicle to exit from the platoon, allowing new vehicles to join the platoon and bringing the platoon to a complete stop at the end of the highway. Test results presented in this paper show that the system was able to perform accurate speed and spacing control and accurate lane keeping as well as provide excellent ride quality comparable to that of extremely good human drivers. The inter-vehicle spacing was maintained to within an accuracy of 20 cm in the case of the eight-car platoon. The switching from brakes to throttle and vice-versa was almost imperceptible to the passengers. The lateral lane keeping was accurate to within 10–cm at all speeds. The algorithms and protocols for lane change and for the split and join maneuvers provided accurate and reliable performance.

Acknowledgment

This work was conducted at the University of California PATH Program, as part of the National Automated Highway Systems Consortium (NAHSC), under cooperative agreement DTFH61-94-X-00 001 with the U.S. Department of Transportation, Federal Highway Administration. The cooperation of the other core participants in the NAHSC is appreciated, particularly that of General Motors Research, Delco Electronics, Delphi Saginaw, Delphi Chassis and Hughes Aircraft Company who developed many of the components on the experimental vehicles. The authors would also like to thank PATH demo-team members B. Bougler, C. Chen, S. Choi, F. Eskafi, J. Guldner, K. Hedrick, S. Mahal, D. Nelson, S. Patwardhan, R. Prohaska, J. Kniffen, P. Kretz, A. Segal and S. Shladover for their contribution and many personal sacrifices.

References

[1] S. B. Choi and J. K. Hedrick, "Vehicle longitudinal control using an adaptive observer for automated highway systems," presented at the Proc. Amer. Contr. Conf., Seattle, WA, 1995.

[2] S. B. Choi and P. Devlin, "Throttle and Brake Combined Control for Intelligent Vehicle Highway Systems," , SAE 951 897, 1995.

[3] J. Guldner, H.-S. Tan, and S. Patwardhan, "Analysis of automatic steering control for highway vehicle with look-down lateral reference systems," *Vehicle Syst. Dynamics*, vol. 26, no. 4, pp. 243–269, 1996.

[4] J. K. Hedrick, D. McMahon, V. K. Narendran, and D. Swaroop, "Longitudinal vehicle controller design for IVHS systems," in *Proc. 1991 Amer. Contr. Conf.*, vol. 3, June 1991, pp. 3107–3112.

[5] J. K. Hedrick, D. McMahon, and D. Swaroop, "Vehicle modeling and control for automated highway systems,", PATH Res. Rep., UCB-ITS-PRR-93-24, 1993.

[6] S. Patwardhan and M. Tomizuka, "Robust failure detection in lateral control for IVHS," in Proc. 1992 Amer. Contr. Conf., June 1992.

[7] R. Rajamani, J. K. Hedrick, and A. Howell, "A complete fault diagnostic system for longitudinal control of automated vehicles," presented at the Proc. Symp. Advanced Automotive Contr., ASME Int. Congr., Nov. 1997.

[8] R. Rajamani and C. Zhu, "Semiautonomous adaptive cruise control," in *Proc. 1999 Amer. Contr. Conf.*, 1999, pp. 1491–1495.

[9] J. J. E. Slotine and W. Li, *Applied Nonlinear Control*. Englewood Cliffs, NJ: Prentice-Hall, 1991.

[10] D. Swaroop and J. K. Hedrick, "String stability of interconnected dynamic systems," *IEEE Trans. Automat. Contr.*, Mar. 1996.

[11] D. Swaroop, J. K. Hedrick, C. C. Chien, and P. Ioannou, "A comparison of spacing and headway control laws for automatically controlled vehicles," *Vehicle Syst. Dynamics J.*, vol. 23, no. 8, pp. 597–625, Nov. 1994.

[12] H. S. Tan, J. Guldner, C. Chen, and S. Patwardhan, "Lane changing on automated highways with look down reference systems," presented at the Proc. IFAC Wshp. Advances in Automotive Contr., Feb. 1998.

[13] M. Tomizuka and J. K. Hedrick, "Automated vehicle control for IVHS systems," in Proc. IFAC Conf., Sydney, NSW, Australia, 1993.

[14] W. B. Zhang and R. E. Parsons, "An intelligent roadway reference system for vehicle lateral guidance/control," in *Proc. Amer. Contr. Conf.*, San Diego, CA, 1990, pp. 281–286.

Rajesh Rajamani (M'94) received the B.Tech. degree from the Indian Institute of Technology, Madras, in 1989, and the M.S. and Ph.D. degrees from the University of California, Berkeley, in 1991 and 1993, respectively.

He worked as a Research Engineer at United Technologies Research Center (UTRC) for three years during which he won the Outstanding Achievement of the Year Award in 1995 for his work on Active Magnetic Guidance of Elevators. From August 1996 to August 1998, he was a Research Engineer with the Automated Highway Systems Program at California PATH, University of California, Berkeley. He is currently Nelson Assistant Professor in the Department of Mechanical Engineering at the University of Minnesota. His research interests include control design and state estimation for nonlinear systems, fault diagnostics, intelligent transportation systems, vibration control and active noise control. He has authored more than 25 publications in journals and conferences, received two patents, and has three other pending patent applications.

Han-Shue Tan received the M.S. and Ph.D. degrees from the University of California, Berkeley, in 1984 and 1988, respectively.

Before joining the California PATH program (University of California at Berkeley) in 1994, he was with the Space and Communication Group, Hughes Aircraft Company, and Hughes Missile Systems Company from 1988 to 1994. His main focus at PATH is on research issues related to vehicle control and vehicle lateral dynamics. His research interests include system dynamics, human/machine interaction and control, linear and nonlinear control theory, and their applications to vehicle as well as to mechanical system control problems.

Boon Kiat Law received the B.Sc. degree in electrical engineering and computer science from University of California, Berkeley, in 1996 and the M.Sc. degree in information networking from Carnegie Mellon University in 1998.

He is currently a Member of Technical Staff at Open Telephone Network, Inc., a telecom start-up in Berkeley, CA, where he works with various telecommunication protocols.

Wei-Bin Zhang is a Research Engineer with University of California (UC), Berkeley, where he has been conducting research on Intelligent Transport Systems and Advanced Vehicle Control and Safety Systems (AVCSS) under the California PATH Program since 1987. From 1994 to 1995, he was the Technical Director of the National Automated Highway Systems Consortium (NAHSC). From 1996 to 1997, he was the Program Manager for the development of the platoon demonstration system for the 1997 AHS demonstration. He is currently managing projects and conducting research in the areas of AVCSS applications for safety and Bus Rapid Transit (BRT) systems.

Prior to Joining UC Berkeley, he was a faculty member of the Northern Jiaotong University, China, where he is still serving as an Adjunct Professor.